



Deposited via The University of Leeds.

White Rose Research Online URL for this paper:

<https://eprints.whiterose.ac.uk/id/eprint/133272/>

Version: Accepted Version

---

**Article:**

Zou, J, Oladipo, J, Fu, S et al. (2018) Hydrogen production from cellulose catalytic gasification on  $\text{CeO}_2/\text{Fe}_2\text{O}_3$  catalyst. Energy Conversion and Management, 171. pp. 241-248. ISSN: 0196-8904

<https://doi.org/10.1016/j.enconman.2018.05.104>

---

(c) 2018, Elsevier Ltd. This manuscript version is made available under the CC BY-NC-ND 4.0 license <https://creativecommons.org/licenses/by-nc-nd/4.0/>

**Reuse**

This article is distributed under the terms of the Creative Commons Attribution-NonCommercial-NoDerivs (CC BY-NC-ND) licence. This licence only allows you to download this work and share it with others as long as you credit the authors, but you can't change the article in any way or use it commercially. More information and the full terms of the licence here: <https://creativecommons.org/licenses/>

**Takedown**

If you consider content in White Rose Research Online to be in breach of UK law, please notify us by emailing [eprints@whiterose.ac.uk](mailto:eprints@whiterose.ac.uk) including the URL of the record and the reason for the withdrawal request.

# Hydrogen production from cellulose catalytic gasification on CeO<sub>2</sub>/Fe<sub>2</sub>O<sub>3</sub> catalyst

Jun Zou<sup>a</sup>, Japhet Oladipo<sup>b</sup>, Shilong Fu<sup>a</sup>, Amal Al-Rahbi<sup>b</sup>, Haiping Yang<sup>a\*</sup>, Chunfei Wu<sup>c\*</sup>, Ning Cai<sup>a</sup>, Paul Williams<sup>b</sup>, Hanping Chen<sup>a</sup>

<sup>a</sup> State Key Laboratory of Coal Combustion, Huazhong University of Science and Technology, Wuhan, 430074, China

<sup>b</sup> School of chemical and process engineering, SCAPE, The University of Leeds, Leeds, LS2 9JT, UK

<sup>c</sup> School of Engineering, University of Hull, Hull, HU6 7RX, UK

\* Corresponding author (H. Yang). Tel.: +86 27 87542417. Email:

yhping2002@163.com

\*\* Corresponding author (C. Wu),. Tel.: +44 1133432504. Email: C.Wu@hull.ac.uk

## Abstract

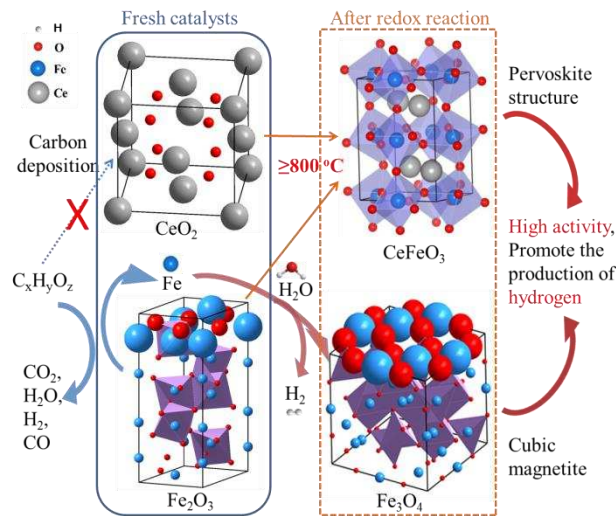
Catalytic steam gasification of biomass can produce clean and renewable hydrogen. In this study, Ce/Fe bimetallic catalysts were used to promote hydrogen production from cellulose steam catalytic reforming at 500-900 °C. The effect of different Ce/Fe ratios on the catalytic performance of hydrogen production was studied. The distribution of products, gas composition, carbon deposition and the stability of the catalyst were analyzed with variant approaches. The results show that the catalytic performance of the CeO<sub>2</sub>/Fe<sub>2</sub>O<sub>3</sub> catalyst in relation to hydrogen production was much better than pure CeO<sub>2</sub> or Fe<sub>2</sub>O<sub>3</sub>. When the ratio of Ce:Fe was 3:7, the maximum yield of the H<sub>2</sub> was 28.58 mmol at 800 °C. CeFeO<sub>3</sub> could be generated at 800 °C or higher temperature

23 after redox reactions without forming  $\text{CeO}_2/\text{Fe}_2\text{O}_3$  clathrate. And the existence of  
24  $\text{CeFeO}_3$  enhanced the thermal stability of Ce/Fe catalyst. The presence of  $\text{CeO}_2$  not  
25 only improved the oxidative ability of the iron catalysts, but also was in favour of the  
26 oxidation of possible deposited carbon on the surface of the used catalysts.

27 Keywords: Hydrogen; Catalytic gasification; Cellulose; Biomass ;  $\text{CeO}_2/\text{Fe}_2\text{O}_3$

28

29



31

32 Schematic of cellulose gasification process with CeO<sub>2</sub>/Fe<sub>2</sub>O<sub>3</sub>. After redox reaction,  
 33 high active phases like CeFeO<sub>3</sub> and Fe<sub>3</sub>O<sub>4</sub> were generated.

34 1. Introduction

35 Hydrogen is a renewable and clean energy carrier and its application only  
 36 generates water [1, 2]. Currently, the production of hydrogen is mainly from the  
 37 processing of fossil fuels such as coal gasification and natural gas reforming. The use  
 38 of fossil fuels results in the generation of greenhouse gases which are responsible for  
 39 climate change. Hence, renewable and sustainable feedstocks such as biomass have  
 40 drawn increasing attention [3, 4]. Converting renewable biomass into hydrogen can be  
 41 processed through steam catalytic gasification [5-8].

42 However, there are many challenges for catalytic biomass gasification. For  
 43 example, the content of alkali metals in biomass is very high, which could be  
 44 evaporated at high temperature and cause corrosion and agglomeration issues [9].  
 45 Another challenge of catalytic biomass gasification is that heavy tar compounds  
 46 produced from thermal-chemical conversion of biomass can cause coke deposition on

47 the surface of catalysts. Considering those two issues, a two-stage pyrolysis-catalytic  
48 steam reforming is proposed and applied [10, 11]. In the two-stage process of biomass  
49 gasification, the pyrolysis of biomass happens at the first stage. And the derived  
50 vapours from biomass gasification are catalytic reformed to produce hydrogen with  
51 catalyst in the second stage. Therefore, the catalytic stage can be separately controlled  
52 with flexible manipulation of process parameters [12, 13]. In addition, the poisoning  
53 of catalyst caused by the contaminants from biomass pyrolysis can be limited [14].

54 Apart from the process optimisation of biomass gasification, catalyst plays an  
55 important role in tar conversion and promoting hydrogen production [10, 11, 14].  
56 Generally, metallic catalysts like nickel or iron based materials perform well in the  
57 thermochemical conversion processes as widely reported [14-17]. Although Fe-based  
58 catalysts offer relatively low activity than Ni, Fe is not toxic and much cheaper.  
59 Therefore, it has high economic feasibility potentials in biomass gasification [18-21].  
60 Furthermore, to reach the goal of turning the gas products into hydrogen enriched  
61 syngas, steam as the gasification oxidant agent is necessary and water gas shift  
62 reaction (WGS) is applied [22-25]. It is known that the efficient catalytic metal for  
63 WGS is  $\text{Fe}_3\text{O}_4$  [24, 26, 27].

64 However, iron catalyst has some disadvantages mainly caused by thermal sintering  
65 of the active phase  $\text{Fe}_3\text{O}_4$  at high gasification temperature [27]. Another problem of  
66 iron catalyst deactivation is caused by the over-reduction of  $\text{Fe}_2\text{O}_3$  to metallic iron and  
67 even iron carbides [28], while the metallic Fe is beneficial for Fischer-Tropsch [29]  
68 and methanation reactions but not helpful to WGS process [30, 31]. So metal oxides

69 supporters like  $\text{Al}_2\text{O}_3$ ,  $\text{Cr}_2\text{O}_3$ ,  $\text{ZrO}_2$  or  $\text{SiO}_2$  were introduced into the iron oxides to  
70 decrease the sintering and enhance the material stability [32]. In the tar reforming  
71 experiments, Kell found that the mixture of La and Fe with  $\text{ZrO}_2$  as support show high  
72 catalytic activity in benzene cracking [21]. While Kang pointed out that the  
73 introducing of copper to  $\text{Fe}_3\text{O}_4$  increased the reduction kinetics and inhibited the  
74 carbon deposition and  $\text{Fe}_3\text{C}$  formation during methane reforming [30]. Khan  
75 introduced several metal ions into the iron oxide and found that the influencing effect  
76 strongly rely on the nature of addition of metal cations, and Fe/Ce could approach  
77 equilibrium conversion during high temperature water gas shift reaction, and ceria  
78 exhibits a synergetic effect on the performance of iron oxide [27]. On the one hand,  
79 some of the researchers focus on the small amount of  $\text{CeO}_2$  with some other metal  
80 oxide as a promoter for tar reforming [16, 17, 22]. Laosiripojana suggested that the  
81  $\text{GdCeO}_2$  coating over  $\text{NiFe/MgOAl}_2\text{O}_3$  performed much better in naphthalene steam  
82 reforming [16]. Chen found that  $\text{La}_{0.8}\text{Ce}_{0.2}\text{FeO}_3$  catalyst showed better activity and  
83 stability than commercial  $\text{Ni/Al}_2\text{O}_3$  during bio-oil/bioslurry steam gasification [22].  
84 On the other hand, to prevent the over-reduction of iron oxide, high capacity and  
85 mobility of oxygen is essential to improve the oxidative ability of the iron catalysts,  
86 and high Ce:Fe ratio catalyst was usually used for oxygen carrier in redox reaction.  
87 Lee found that Fe-based mediums with 30 wt% of  $\text{CeO}_2$  exhibited high activity and  
88 stability in water splitting oxidation for chemical hydrogen storage [33]. And Fe/Ce  
89 performed well in Reddy's the long-term water gas shift reaction experiments.  
90 Yamaguchi also pointed out that  $\text{CeO}_2$  was an effective modification of  $\text{Fe}_2\text{O}_3$  and

91 improved the thermal stability during the methane-steam redox process [34]. However,  
92 biomass steam gasification is much more complex than oil model compounds  
93 gasification and water-gas shift or other simple gas like methane steam reforming; it  
94 includes all above reactions and is consisted of volatile releasing, cracking and  
95 derived gases steam reforming. So the influence of Ce/Fe catalyst in biomass steam  
96 gasification should be explored.

97 In addition, the application about perovskite structure( $ABX_3$ ) in photochemical  
98 reactions has been drawn more and more attentions since it was rated the top 10  
99 scientific breakthroughs by the editors Science [35] and Nature [36] in 2013.  
100 Moreover, relatively high ratio of  $CeO_2$  in Ce/Fe catalyst has been synthesised into  
101  $CeFeO_3$ , whose perovskite structure exhibits not only high photocatalytic activity [37],  
102 but also high capacity and mobility of oxygen, which means that it is potential to be  
103 used in redox process [38-40]. Manwar revealed that nanocrystalline  $CeFeO_3$  is a  
104 potential candidate for photo-electrochemical water splitting reaction [41]. However  
105 they are seldom studied in thermal-chemical reactions. Recently, Sahoo synthesized 3  
106 or 6 at.% Fe-doped  $CeO_2$  with microwave assisted combustion method and found that  
107 they could be used for both CO oxidation and soot combustion, and exhibited high  
108 thermal stability [42]. Ce/Fe binary catalysts have been studied by introducing high  
109 ratio of ceria into the catalyst to forming  $CeFeO_3$  rather than acting as catalyst  
110 supporter or promoter. In addition, these catalysts were used mainly for  
111 photochemical reaction rather than for biomass steam gasification. This paper uses  
112 high photocatalytic active phase of  $CeFeO_3$  for biomass steam gasification.

113        Thereby, in this study, Ce/Fe catalyst was introduced into biomass steam  
114        gasification and optimizing the mole ratio of cerium to iron is studied, in relation to  
115        the yield of hydrogen production and the stability of catalyst using a two-stage reactor.  
116        Temperature programmed reduction/oxidation (TPR/TPO) and X-Ray Diffractometer  
117        (XRD) were applied to investigate the formation of CeFeO<sub>3</sub> and the mechanism of the  
118        CeO<sub>2</sub>/Fe<sub>2</sub>O<sub>3</sub> catalysts on biomass gasification.

119

## 120        2. Experimental material and methods

### 121        2.1 Biomass materials and catalyst preparation

122        Cellulose (microcrystalline powders of 20 μm particle size, Sigma-Aldrich Co.,  
123        Ltd.) was applied as a representative material of biomass feedstock. Proximate and  
124        ultimate analysis of the cellulose sample can be found in our previous work [43]. The  
125        TGA analysis showed that cellulose began to decompose at about 310 °C and was  
126        entirely converted at 450 °C, as shown in supplementary materials Fig.1S.

127        A wet impregnation method was applied for the preparation of CeO<sub>2</sub>/Fe<sub>2</sub>O<sub>3</sub>  
128        catalysts. CeO<sub>2</sub> (analytically pure, Sigma-Aldrich Co., Ltd.) was impregnated with  
129        aqueous solution of Fe(NO<sub>3</sub>)<sub>3</sub>•9H<sub>2</sub>O (analytically pure, Sigma-Aldrich Co., Ltd.). The  
130        catalyst precursors were kept stirring at 80 °C for 6h and dried at 105 °C overnight,  
131        and subsequently calcined at 800 °C for 4h in a muffle furnace under air atmosphere.  
132        Then the catalysts were crushed and sieved to granules with the size ranging from  
133        0.245 to 0.350 mm prior to experimental work. While the raw CeO<sub>2</sub> and Fe<sub>2</sub>O<sub>3</sub>  
134        (analytically pure, Sigma-Aldrich Co., Ltd.) were used directly as catalysts for

135 comparison. The catalysts were not reduced prior to the experiment since the derived  
136 gases during pyrolysis-gasification process like hydrogen and carbon monoxide can  
137 reduce the metal oxides in situ. Different mole ratios of Ce/Fe in  $Ce_xFe_yO$  were  
138 prepared as X:Y=1:0, 7:3, 5:5; 3:7; 0:1. The actual ratios of Ce:Fe after the  
139 preparation of catalysts were detected by ICP-MS (ELAN DRC-e, PerkinElmer,  
140 America), and the related results were listed in Table 1S. The blank experiment  
141 without any catalysts was assigned as “w/o”.

142

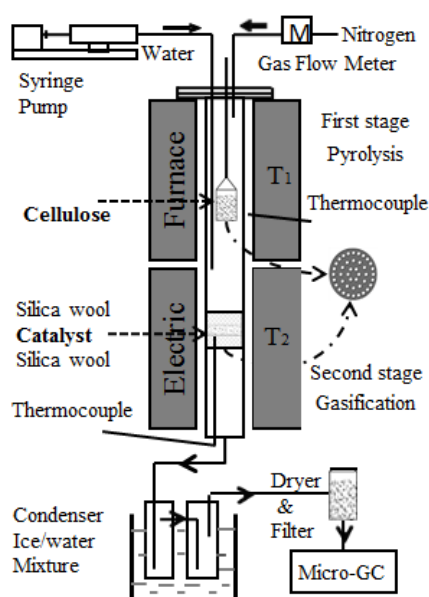
## 143 2.2 Experiment apparatus and method

144 The gasification of cellulose sample was performed in a two stage pyrolysis  
145 catalytic reforming fixed-bed system as shown in Fig. 1, which is consisted of  
146 two-stage fixed-bed furnace with two temperature ranges (First stage: pyrolysis zone;  
147 Second stage: gasification zone; the height of both is 310 mm ), a quartz tube reactor  
148 with an internal diameter of 45 mm, water feeding system, cooling system filled with  
149 water/ice mixture, as well as gas cleaning system following by gas collecting and  
150 measuring system.

151 For each experiment, 1 g  $CeO_2/Fe_2O_3$  catalyst, embraced by quartz wool, was put  
152 on a porous plate in the second reactor. The carrier gas (Nitrogen, 99.999%) was kept  
153 as  $300\text{ ml min}^{-1}$ . Then the first stage was set at  $800\text{ }^\circ\text{C}$  for cellulose pyrolysis, while  
154 the gasification temperature varied from  $500\text{ }^\circ\text{C}$  to  $900\text{ }^\circ\text{C}$  with the step of  $100\text{ }^\circ\text{C}$ .  
155 When the pyrolysis and gasification reactors were heated and stabilized at set  
156 temperatures, respectively, 2 g cellulose (supported by silica wool, in a quartz basket

157 with an internal diameter of 28 mm) was fed into the first reactor. At the same time, a  
158 precise syringe pump introduced the water at  $0.1 \text{ g min}^{-1}$  through a stainless steel tube  
159 which passed the pyrolysis stage and reached the entrance of gasification reactor for  
160 catalytic steam reforming. Fast pyrolysis of cellulose sample happened in the first  
161 stage and the derived pyrolyzed volatiles were catalytic steam reformed at the second  
162 stage in the presence of the  $\text{CeO}_2/\text{Fe}_2\text{O}_3$  catalyst. After the pyrolysis and catalytic  
163 reforming, the outlet products passed through two condensers with water ice mixture,  
164 where the water and condensable vapors were collected. Finally, the noncondensable  
165 gases were cleaned, dried and sampled with a gas bag. The gas sample was collected  
166 every two minutes for detecting the gas content. It turned out that the effective gases  
167 like  $\text{CO}$ ,  $\text{H}_2$ ,  $\text{CO}_2$  and  $\text{CH}_4$  were below detection limit after 40 minutes, so it can be  
168 sure that the reaction was completed and all the products were collected. Each  
169 experiment was performed for 40 minutes and every gas sample was tested for three  
170 times at least and the results were averaged.

171



172

173 Figure 1. Schematic diagram of the reactor system

174 2.3 Characterizations of gas products and catalysts

175 Gas sample collected in the gas bag was analyzed off-line with a gas  
176 chromatography (GC) (Panna A91, China). The produced gas sample was analyzed  
177 using a dual channel GC with a thermal conductivity detector (TCD) and a flame  
178 ionization detector (FID). Column A was Porapak Q (He as carrier gas) for the  
179 analysis of CO<sub>2</sub> at 80°C. Column B was 5A zeolite molecular sieve (MS-5A, He as  
180 carrier gas) for the measurement of H<sub>2</sub>, N<sub>2</sub>, O<sub>2</sub>, CO, CH<sub>4</sub> at 100°C. The N<sub>2</sub>  
181 concentration and flow rate were used as the tracer to calculate the mass of each gas  
182 (in volume, at 1 atm and 25°C). The total yield of gas production and liquid  
183 production were calculated by the obtained mass of gas and liquid in relation to the  
184 weight of cellulose sample. And the variation of char yield can be neglected since the  
185 pyrolysis stage was carried out at the same condition at each experiment and the  
186 weight of residual solid char ranged from 0.119 g to 0.121 g. While the mass balance  
187 was calculated by that the whole productions of gas, liquid and char divided by the  
188 total weight of input including cellulose and steam. For each test, it was repeated at  
189 least three times, the repeatability was kept above 95%, and the results were averaged.

190 In order to investigate the stability performance of the catalysts during the cellulose  
191 gasification, life time test was carried out. After each experiment, the catalyst was  
192 kept in the furnace without any other changing while just the fresh cellulose sample  
193 was introduced. So the used catalyst was recycled for the cellulose catalytic  
194 gasification.

195 The crystal structure of the fresh and used catalysts was characterized by X-Ray  
196 Diffractometer (XRD, X'Pert PRO, PANalytical B.V, Netherlands) with Cu K $\alpha$   
197 radiation ( $\lambda=1.5406 \text{ \AA}$ ) operating at 40KV and 40mA at  $2\theta$  range between 10 and 85°.  
198 PANalytical X'pert HighScore software was used to analyse the diffraction spectra  
199 peaks and the reference data from the Joint Committee on Powder Diffraction  
200 Standard (JCPDS) files was applied to identify the crystal phases existed in the  
201 samples.

202 The reducibility of the catalysts was characterized with Hydrogen temperature  
203 programmed reduction method (H<sub>2</sub>-TPR) using a Catalyst Analyzer (Belcat-M,  
204 Microtrac BEL., Corp). Before the reduction, 100 mg catalyst was heated from room  
205 temperature to 500 °C at a heating rate of 10 °C min<sup>-1</sup> and kept isothermal for 1h, then  
206 cooled down to 100 °C. In the above process, High purity argon (99.999%) was used  
207 as purging gas. After that the gas was switched to 5% H<sub>2</sub>/Ar (30 cm<sup>3</sup> min<sup>-1</sup>), the TPR  
208 test was carried out from 100 °C to 800 °C at a heating rate of 10 °C min<sup>-1</sup> and kept  
209 for 30 minutes. An on-line thermal conductivity detector (TCD) was applied to  
210 measure the consumption of hydrogen [44].

211 In order to investigate the properties of used catalysts and the possible deposited  
212 carbon on the surface, temperature programmed oxidation (TPO) was carried out in a  
213 thermogravimetric analyser (Labsys Evo1150, Setaram instrumentation, France). 30  
214 mg reacted catalyst was heated to 105 °C and kept for 20 minutes, then it was heated  
215 up to 850 °C at 10 °C min<sup>-1</sup>, and holding for 20 minutes. A high resolution scanning

216 electron microscope (SEM, Quanta 200, FEI, Netherlands) was applied to test the  
217 surface morphology of the used catalysts.

### 218 3. Results and discussion

#### 219 3.1. Influence of the ratio of Ce:Fe

##### 220 3.1.1. Gas distribution

221 To investigate the influence of the ratio of Ce:Fe on the cellulose steam  
222 gasification, pure CeO<sub>2</sub> or Fe<sub>2</sub>O<sub>3</sub> and different mole ratios of Ce:Fe (7:3, 5:5, 3:7)  
223 were introduced into the catalytic stage. Both pyrolysis stage and gasification stage  
224 were set at 800 °C. And the feeding rate of water was kept at 0.1 g min<sup>-1</sup>. Since the  
225 reaction time was 40 min, the total water introduced into the system was 4 g, which  
226 far surpassed the content of tar in the liquid product (water and tar were both  
227 condensed in the condenser), the characteristics of oil was not analyzed here. And the  
228 weight of residual solid char was steady from 0.119 g to 0.121 g, which indicated that  
229 the variation of char yield could be neglected since the pyrolysis stage was carried out  
230 at the same condition for each trial. While the total yield of gas production was  
231 calculated with the mass of gas in relation to the weight of cellulose sample. And the  
232 product yield and gas distribution of cellulose gasification with variant Ce/Fe catalyst  
233 are shown in Table 1. The mass balance was calculated by that the whole productions  
234 of gas, liquid and char divided by the total weight of input including cellulose and  
235 steam, and its' value ranged from 96.54% to 100.15%, it indicated that the experiment  
236 results were reliable. Under the condition that without any catalysts were used, the gas  
237 yield was 71.53 wt%, while the yield and content of hydrogen were 13.88 mmol g<sup>-1</sup>

238 cellulose and 23.07 vol.% separately, the values of them were low. When CeO<sub>2</sub> was  
239 introduced, the gas yield was decreased slightly from 71.53 wt.% to 70.45 wt.% but  
240 the yield of hydrogen was increased slightly to 15.65 mmol g<sup>-1</sup> cellulose, while the  
241 content of CO<sub>2</sub> decreased sharply and the content of CO increased significantly, this might be  
242 attributed to that CeO<sub>2</sub> prevented the further conversion of oil and the water gas shift. In  
243 regard to Fe<sub>2</sub>O<sub>3</sub> addition, the same tendency was showed with that of CeO<sub>2</sub>. The CO content  
244 increased up to 53.07 vol.% at the price of CO<sub>2</sub> diminishing to 10.42 vol.%. The content of H<sub>2</sub>  
245 was decreased slightly from 23.07 vol.% to 22.05 vol.%, while the yield of hydrogen  
246 increased to 17.30 mmol g<sup>-1</sup> cellulose. However, the gas yield under Fe<sub>2</sub>O<sub>3</sub> increased largely  
247 to 87.13% which is much higher than that of CeO<sub>2</sub>. It indicated that Fe<sub>2</sub>O<sub>3</sub> performed  
248 important role in promoting the thermal cracking and steam reforming of tar into light gases.  
249 In general, the yield of combustible gases (H<sub>2</sub>, CO, CH<sub>4</sub>) increased when CeO<sub>2</sub> or  
250 Fe<sub>2</sub>O<sub>3</sub> was introduced. And the low heating value was 13.55 MJ (Nm<sup>3</sup>)<sup>-1</sup> and 14.27MJ  
251 (Nm<sup>3</sup>)<sup>-1</sup> respectively.

252 The yield of gas product with CeO<sub>2</sub>/Fe<sub>2</sub>O<sub>3</sub> mixture was shown in Table 1. With the  
253 ratio of Fe increasing, the concentration of CO increased slightly from 49.15 vol.% to  
254 53.07 vol.% ( the yield of CO was increased by 34.5% from 30.97 mmol to 41.64  
255 mmol correspondingly, refer to Fig.2S), CH<sub>4</sub> showed similar trend as the content of  
256 CH<sub>4</sub> was increased slightly from 12.99 vol.% to 14.45 vol.%, while the CO<sub>2</sub>  
257 concentration decreased from 13.00 vol.% to 10.42 vol.%. It is suggested that the  
258 introduction of Fe promoted the thermal cracking of the pyrolysis volatiles resulting  
259 in the increase of the production of CO and CH<sub>4</sub>. It should be noticed that when the

260 ratio of Ce:Fe was decreased gradually from 1:0 (pure CeO<sub>2</sub>) to 0:1 (pure Fe<sub>2</sub>O<sub>3</sub>), the  
 261 concentration of H<sub>2</sub> and CO<sub>2</sub> were increased initially and then reduced, while the  
 262 concentration of CO was decreased at first and then increased. Those might be related  
 263 to reverse water gas shift (RWGS, CO<sub>2</sub> + H<sub>2</sub> = CO + H<sub>2</sub>O, ΔH = +41.19 KJ mol<sup>-1</sup>),  
 264 which was endothermic reaction. It is proposed that the reverse water gas shift at 800  
 265 °C was enhanced, which restrained the production of H<sub>2</sub> and CO<sub>2</sub>. The maximum  
 266 yield of hydrogen (28.58 mmol, more than twice of without catalyst) was obtained at  
 267 the Ce:Fe ratio of 3:7. It indicates that the ratio of 3:7 (Ce:Fe) is the optimal value  
 268 for the hydrogen production in this work, much better than that of pure CeO<sub>2</sub> or Fe<sub>2</sub>O<sub>3</sub>.  
 269 It might be owing to that ceria and iron shows synergy in volatile conversion and  
 270 hydrogen production.

271 Table.1 Gas yields under different mole ratios of Ce:Fe.

Different Ce:Fe ratio	w/o	CeO <sub>2</sub>	Ce:Fe=7:3	Ce:Fe=5:5	Ce:Fe=3:7	Fe <sub>2</sub> O <sub>3</sub>
Gas yield (wt.%)	71.53	70.45	74.36	83.79	84.64	87.13
Mass balance (%)	98.74	100.15	96.54	98.90	98.30	98.28
H <sub>2</sub> yield (mmol g <sup>-1</sup> cellulose)	13.88	15.65	21.70	27.01	28.58	17.30
Gas composition (vol.%)						
H <sub>2</sub>	23.07	24.85	30.38	32.53	33.69	22.05
CO <sub>2</sub>	20.57	13.00	13.70	12.77	12.12	10.42
CH <sub>4</sub>	12.79	12.99	12.65	13.20	10.93	14.45
CO	43.58	49.15	43.27	41.50	43.26	53.07

272

### 273 3.1.2. XRD analysis

274 Fig. 2 shows the X-ray diffraction patterns of the fresh and reacted catalysts with  
 275 different Ce:Fe ratios prepared by impregnation. It shows that the main crystal phases  
 276 in the fresh catalysts were the same, it mainly includes Fe<sub>2</sub>O<sub>3</sub> (Rhombohedral

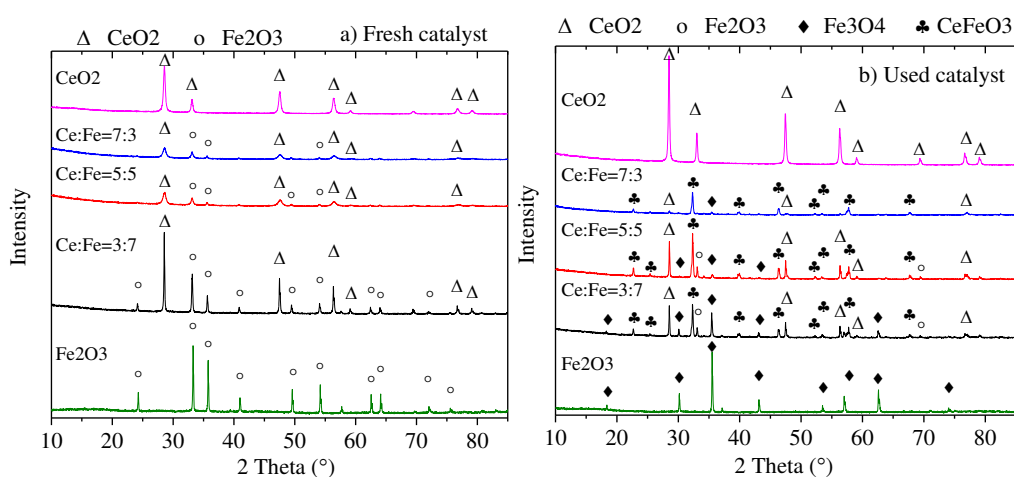
277 hematite phase, JCPDS 00-001-1053) and/or CeO<sub>2</sub> (cubic phase, JCPDS  
278 01-081-0792). As for the pure CeO<sub>2</sub> catalyst, the XRD patterns before and after  
279 reaction showed similar crystal phases, although the crystallinity was increased after  
280 experiments. While the peaks of pure Fe<sub>2</sub>O<sub>3</sub> was totally disappeared, Fe<sub>3</sub>O<sub>4</sub> (cubic  
281 magnetite phase, JCPDS 00-001-1111) were observed after the redox reactions. It  
282 might be attributed that the presence of reducing gases (e.g. H<sub>2</sub> and CO) reduced the  
283 Fe<sub>2</sub>O<sub>3</sub> catalysts into compounds such as Fe<sub>3</sub>O<sub>4</sub> which was the active phase in water  
284 gas shift process. While the metallic Fe<sup>0</sup> was not observed in the XRD patterns. It  
285 might be owing to that the Fe<sup>0</sup> was oxidized to Fe<sub>3</sub>O<sub>4</sub> by steam ( $3\text{Fe} + 4\text{H}_2\text{O} (\text{vapor}) =$   
286  $\text{Fe}_3\text{O}_4 + 4\text{H}_2$ ), since the steam was fed to the system continuously. Fe<sup>0</sup> in iron oxygen  
287 carrier could not be fully oxidized into Fe<sup>3+</sup> with steam as oxidizing agent, this is in  
288 agreement with Vozniuk's work [45]. Therefore, Fe<sub>3</sub>O<sub>4</sub> was identified in the XRD  
289 patterns of the used Fe<sub>2</sub>O<sub>3</sub> catalyst after a series reaction as  $\text{Fe}_2\text{O}_3 \rightarrow \text{Fe}_3\text{O}_4 \rightarrow \text{Fe} \rightarrow$   
290 Fe<sub>3</sub>O<sub>4</sub>.

291 In regard to fresh CeO<sub>2</sub>/Fe<sub>2</sub>O<sub>3</sub> bimetal catalysts, it was noticed that cerium and  
292 iron did not form any binary metal oxides (Ce<sub>x</sub>Fe<sub>y</sub>O), and no obvious phase changes  
293 for Ce and Fe with the ratio of Ce:Fe changing. In addition, there were no cerium/iron  
294 ions substituting into the cerium/iron lattice sites. Since the catalysts were calcined at  
295 800 °C under air environment, Ce<sup>3+</sup> ion was oxidized into Ce<sup>4+</sup> ion, that's the reason  
296 that the diffraction peaks of CeO<sub>2</sub> rather than Ce<sub>2</sub>O<sub>3</sub> exist. With the decrease of the  
297 ratio of Ce:Fe from 7:3 to 5:5 and then 3:7, the content of iron in the mixture was  
298 increased. The diffraction of the fresh catalysts appears to be narrower and sharper

299 when the ratio of Ce:Fe was decreased. Furthermore, the diffraction peaks of Fe<sub>2</sub>O<sub>3</sub>  
300 become more and more obvious especially in the Ce:Fe=3:7 catalyst. It is  
301 demonstrated that the size of metal particles in the prepared catalysts was increased as  
302 evaluated using the Scherrer Equation. In addition, the addition of Fe resulted in the  
303 increase of the crystallinity and the size of Fe-based particles. It can be noticed that  
304 the diffraction peaks of CeO<sub>2</sub> become narrower and sharper as the ratio of ceria in  
305 Ce:Fe decreasing, that indicated the particle sizes of CeO<sub>2</sub> is increasing, it seems that  
306 CeO<sub>2</sub> might be sintering when the amount of CeO<sub>2</sub> atoms is the minority(in this  
307 experiment the ratio of Ce:Fe is 3:7).

308 For the used Ce/Fe catalysts, a perovskite type composite oxide CeFeO<sub>3</sub>  
309 (orthorhombic phase, JCPDS 00-022-0166) and Fe<sub>3</sub>O<sub>4</sub> (cubic magnetite phase,  
310 JCPDS 00-001-1111) were showed. It might be attributed that the presence of  
311 reducing gases (e.g. H<sub>2</sub> and CO) reduced the catalysts into compounds such as Fe<sub>3</sub>O<sub>4</sub>  
312 during the water-shifting process. The new perovskite phase CeFeO<sub>3</sub> was also formed  
313 during the experiment and it has been proved that perovskite ferrite have high  
314 capacity and mobility of oxygen, fast response time and high activity [38], which  
315 might be favourable for cellulose gasification. Unlike only Fe<sub>3</sub>O<sub>4</sub> peaks could be seen  
316 in the used pure Fe<sub>2</sub>O<sub>3</sub> catalyst, both Fe<sub>2</sub>O<sub>3</sub> and Fe<sub>3</sub>O<sub>4</sub> were observed in the used  
317 Ce/Fe catalysts. It could be related to that the introducing of CeO<sub>2</sub> promoted the  
318 oxidation of Fe<sub>3</sub>O<sub>4</sub> to Fe<sub>2</sub>O<sub>3</sub> in steam environment, because ceria has a high and multi  
319 valence state and can undergo fast and reversible Ce<sup>+3</sup> ↔ Ce<sup>+4</sup> transformation for  
320 oxygen storing and releasing.

321 As shown in Fig. 2b, the CeFeO<sub>3</sub> peaks are much more obviously than that of  
 322 Fe<sub>3</sub>O<sub>4</sub> and the peaks of Fe<sub>2</sub>O<sub>3</sub> can't be seen especially at the ratio of Ce:Fe=7:3, i.e.,  
 323 Fe was mainly existed in the form of CeFeO<sub>3</sub> lattice. It is indicated that the Fe  
 324 element in the fresh catalysts was likely to form CeFeO<sub>3</sub> in used catalysts rather than  
 325 Fe<sub>3</sub>O<sub>4</sub> or Fe<sub>2</sub>O<sub>3</sub> after the redox reactions. With Fe ratio increasing, the diffraction peak  
 326 of Fe<sub>3</sub>O<sub>4</sub> is becoming more significant, it can be related to the generated hydrogen and  
 327 carbon monoxide in-situ reduced the iron oxide and the iron-steam reaction (Fe + H<sub>2</sub>O  
 328 = Fe<sub>3</sub>O<sub>4</sub> + H<sub>2</sub>). In return, it promoted the production of CO, H<sub>2</sub> and other gases as  
 329 shown in Table 1, because Fe<sub>3</sub>O<sub>4</sub> was the active phase and had a high catalytic activity.  
 330 And the existence of CeFeO<sub>3</sub> was also beneficial to steam gasification of volatile  
 331 further increasing the gas production than that of pure Fe<sub>2</sub>O<sub>3</sub> or CeO<sub>2</sub>. The hydrogen  
 332 yield reached the maximum with the Ce:Fe=3:7 catalyst which shows strong  
 333 diffraction of CeFeO<sub>3</sub> and Fe<sub>3</sub>O<sub>4</sub> in the XRD analysis.

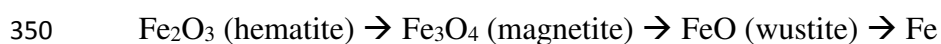


334  
 335 Figure 2. XRD patterns of catalysts with different Ce/Fe ratio.

336

337 3.1.3. TPR (Temperature programmed reduction) analysis

338 Fig. 3 shows the TPR profiles of catalyst reduction in relation to the reduction  
339 stages and the corresponding temperature. For CeO<sub>2</sub>, the reduction of CeO<sub>2</sub> to Ce<sub>2</sub>O<sub>3</sub>  
340 shows two peaks, one quite weak peak at 511.2 °C as the surface shell reduction[27]  
341 (as shown in Fig. 2S) and a relatively slight increase showed at higher temperature  
342 (>700°C) for bulk reduction, it indicated that CeO<sub>2</sub> is very stable, and higher  
343 temperature might lead to the reduction of CeO<sub>2</sub> to Ce<sub>2</sub>O<sub>3</sub>. While Fe<sub>2</sub>O<sub>3</sub> showed good  
344 reducibility, and the reduction process can be divided into 3 steps of reduction. The  
345 reduction of Fe<sub>2</sub>O<sub>3</sub> (hematite) to magnetite (Fe<sub>3</sub>O<sub>4</sub>) was located at ~467.9 °C, and is  
346 followed by the reduction of magnetite (Fe<sub>3</sub>O<sub>4</sub>) to wustite (FeO) at 600 °C ~720 °C.  
347 Further reduction of wustite to metallic Fe<sup>0</sup> happens at around 800 °C, while the  
348 complete reduction of FeO to Fe<sup>0</sup> could not be observed. The process can be  
349 described as the follows:



351 While the reduction of Fe<sub>3</sub>O<sub>4</sub> to FeO as shown in Fig.3 was shifted to higher  
352 temperature and mixed together with the reduction of FeO to Fe<sup>0</sup>. It indicated that the  
353 Fe<sub>3</sub>O<sub>4</sub> was thermal sintering at high temperature and hard to be reduced, as reported in  
354 other's work[46, 47].

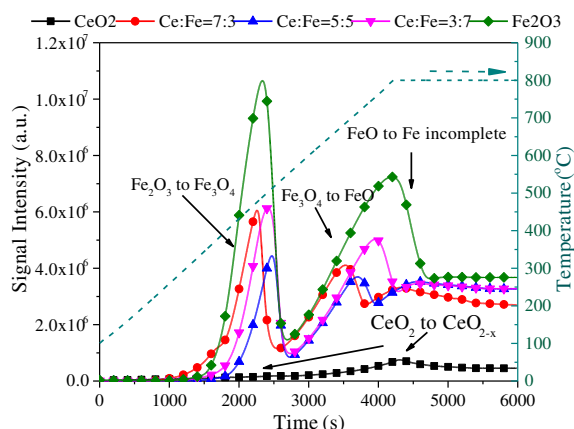
355 Studies show that the reduction process significantly depends on the existence of  
356 another metal oxide in the modified iron oxide[27, 31]. And that is confirmed in  
357 Ce/Fe catalysts. For the mixture of CeO<sub>2</sub> and Fe<sub>2</sub>O<sub>3</sub> (Ce: Fe=7: 3), still three peaks are  
358 showed: i) the reduction of hematite to magnetite at 455.9 °C which is similar with  
359 that of pure Fe<sub>2</sub>O<sub>3</sub>; ii) followed by the reduction of magnetite to wustite which is

360 shifted to lower temperature as 668.8 °C, it means that Fe<sub>3</sub>O<sub>4</sub> is easier to be reduced to  
361 FeO, which indicates that the presence of CeO<sub>2</sub> decreases the thermal sintering of  
362 Fe<sub>3</sub>O<sub>4</sub>; iii) while the last peak was much wider than that of the reduction of wustite to  
363 metallic Fe<sup>0</sup> for pure Fe<sub>2</sub>O<sub>3</sub> catalyst, it might be the combination peaks of the  
364 reduction of CeO<sub>2</sub> to Ce<sub>2</sub>O<sub>3</sub> and FeO to Fe<sup>0</sup>.

365 With the ratio of increasing of Fe (Ce:Fe=5:5), the TPR profile is similar to that  
366 of Ce:Fe=7:3 except that the peak value is lowered and reducibility is weakened. While  
367 with the ratio of Fe increasing further to Ce:Fe=3:7, the reduction of Fe<sub>3</sub>O<sub>4</sub> to FeO  
368 was shifted to high temperature as 706.6 °C obviously, i.e., the reduction of Fe<sub>3</sub>O<sub>4</sub>  
369 became difficult. It might be owing to that the preventing of Fe<sub>3</sub>O<sub>4</sub> from thermal  
370 sintering was weakened as the ratio of CeO<sub>2</sub> was lowered (Ce:Fe=3:7).

371 As can be seen in the TPR results, similar reduction peaks are obtained for Ce/Fe  
372 catalysts and the catalyst with pure CeO<sub>2</sub> or Fe<sub>2</sub>O<sub>3</sub>. Therefore, the possible  
373 intermediate cerium iron bimetallic species is not shown, it suggested that the  
374 interaction between Fe and CeO<sub>2</sub> support was weak after the calcination during the  
375 process of catalysts preparation. This is in good agreement with the XRD results.  
376 However, the reducibility of the catalysts changes with the variation ratio of Ce:Fe,  
377 the reducibility of Ce<sub>3</sub>Fe<sub>7</sub>O<sub>y</sub> is the strongest among the impregnation Ce/Fe catalysts  
378 and surpassed only by pure Fe<sub>2</sub>O<sub>3</sub>, and the whole reduction profile of the CeO<sub>2</sub> shows  
379 that the reducibility of CeO<sub>2</sub> is much less by orders of magnitude than the Ce/Fe  
380 catalysts. This is in positive correlation with the ratio of iron. And the hydrogen  
381 consumption of Fe<sup>3+</sup> → Fe<sup>0</sup> is 26.86 mmol g<sup>-1</sup>, much higher than that of Ce<sup>4+</sup> → Ce<sup>3+</sup>

382 with the value of 3.57 mmol g<sup>-1</sup>.



383

384 Figure 3. TPR profiles of fresh catalysts with different Ce/Fe ratio.

385

### 386 3.2 Lifetime test of the catalysts

387 In order to further investigating the performance of the catalysts during the  
388 gasification of cellulose, the stability of catalysts was tested for 5 cycles (during each  
389 cycle, fresh cellulose sample was introduced) with Ce:Fe=3:7 catalyst used as the  
390 catalyst showed the best performance in terms of hydrogen production. In addition,  
391 the temperature was set as 800°C and the water feeding rate was 0.1 g min<sup>-1</sup> for the  
392 lifetime test. The gas yield was listed in in Table 2. It can be found that when the  
393 catalyst was used for 1 and 2 times, the gas yield increased obviously and the content  
394 of H<sub>2</sub> was kept steady, hence the yield of hydrogen increased gradually to 29.35 mmol  
395 g<sup>-1</sup> cellulose, the performance of catalyst seems to become better and it might be  
396 owing to the existence of highly-active compounds such as Fe<sub>3</sub>O<sub>4</sub> or CeFeO<sub>3</sub> after the  
397 first redox experiment (as shown in Fig.4). However, with catalyst used further (over  
398 3 times), the increasing trend become gentle and H<sub>2</sub> and CO yield decreased slightly,  
399 but CH<sub>4</sub> and CO<sub>2</sub> increased slightly, although the increase of CO<sub>2</sub> (from 10.28 to

400 14.58 mmol g<sup>-1</sup> cellulose) surpassed that of CH<sub>4</sub> (from 9.27 to 11.54 mmol g<sup>-1</sup>  
 401 cellulose) and occupied the main increment. It infers that the oxidation of catalyst  
 402 might be increased and promote the formation of carbon dioxide. However, from the  
 403 life test result, we can know that the yield of H<sub>2</sub> is still kept 26.29 mmol g<sup>-1</sup> with H<sub>2</sub>  
 404 content over 30% and CO about 40%. The heat value is kept at about 13 MJ (Nm<sup>3</sup>)<sup>-1</sup>.  
 405 It indicated that the catalytic activity of the catalyst we used is still kept stable without  
 406 obvious inactivation. It indicated that the performance of Ce:Fe=3:7 catalyst is not too  
 407 bad for hydrogen production after five times reusing test.

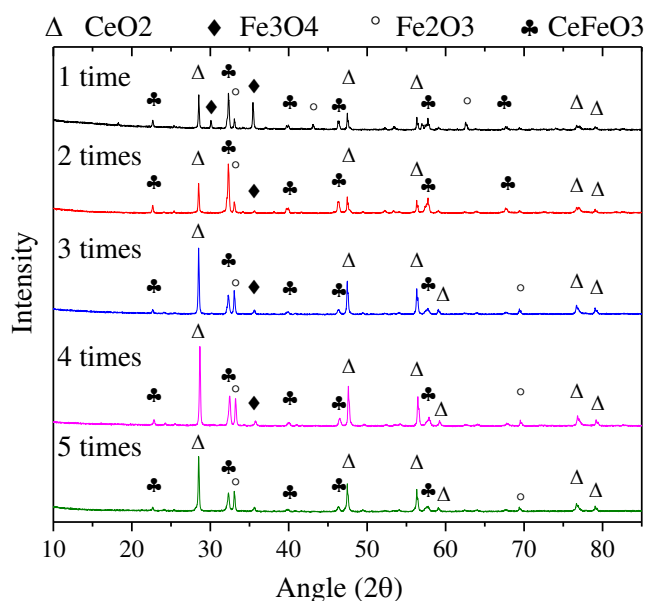
408 Table 2. Gas yields in lifetime test for catalysts (Ce:Fe=3:7) stability.

Life time	1	2	3	4	5
Gas yield (wt.%)	84.64	88.94	90.99	91.50	91.98
Mass balance (%)	98.30	97.99	97.18	96.33	96.16
H <sub>2</sub> yield (mmol g <sup>-1</sup> cellulose)	28.58	29.35	28.12	27.31	26.29
Gas composition (vol.%)					
H <sub>2</sub>	33.69	33.35	31.93	31.17	30.33
CO <sub>2</sub>	12.12	14.23	15.32	15.95	16.81
CH <sub>4</sub>	10.93	11.72	12.48	13.12	13.31
CO	43.26	40.70	40.27	39.75	39.54

409

410 The XRD spectra of used Ce/Fe catalyst is shown in Fig. 4. The XRD spectra  
 411 of the catalyst used with variant cycles exhibit the same pattern. However, the  
 412 diffraction peaks of CeO<sub>2</sub> and Fe<sub>2</sub>O<sub>3</sub> become more and more significant while the  
 413 patterns of CeFeO<sub>3</sub> and Fe<sub>3</sub>O<sub>4</sub> seem to be weakened with the catalyst recycle except  
 414 that there is an increasing of CeFeO<sub>3</sub> peak during the 2 times reusing. It is consistent  
 415 with the catalytic activity as higher H<sub>2</sub> yield for catalyst reused for twice, it indicated  
 416 that Ce<sub>2</sub>FeO<sub>3</sub> is more active for water shifting reaction of biomass with more H<sub>2</sub> and

417 CO formed. The decrement of active compounds of  $\text{CeFeO}_3$  and  $\text{Fe}_3\text{O}_4$  resulted in the  
418 weak performance of catalyst with catalyst reused further (recycle time over 3), while  
419 the increment of  $\text{CeO}_2$  and  $\text{Fe}_2\text{O}_3$  promoted the oxidation of catalyst, and leading to  
420 more  $\text{CO}_2$  formed.

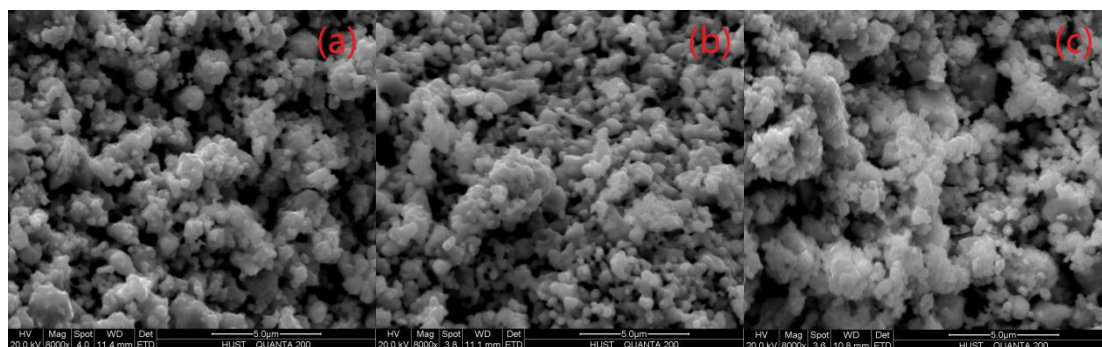


421

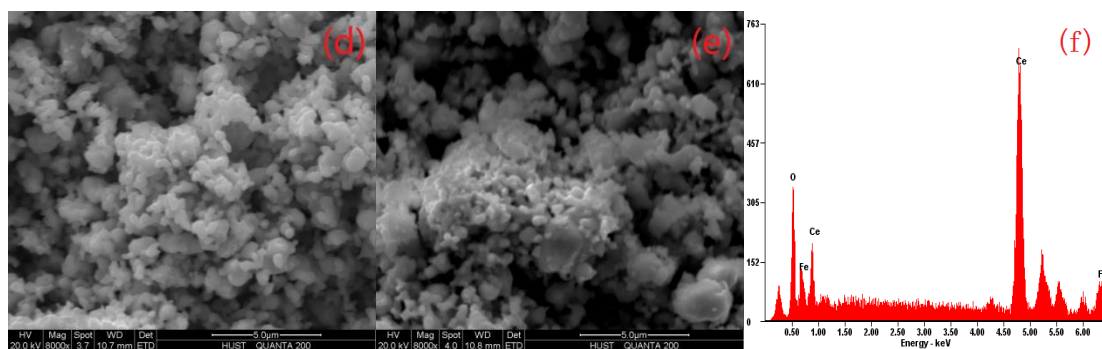
422 Figure 4. XRD patterns of reacted catalysts (Ce:Fe=3:7) after several times.

423 The morphologies of the used catalysts after each cycle were shown in Fig. 5.  
424 The deposition of carbon on the surface of the reacted catalysts is difficult to be  
425 observed as shown in Fig.5, as steam injecting during water-gas shifting process  
426 might react with potential carbon deposition. With catalyst recycle going, some  
427 irregular particles were observed on the surface of catalysts, it might be attributed to  
428 the agglomeration generated at higher temperature (800 °C). Combined with the XRD  
429 results of the reacted catalyst in Fig.4, it might be  $\text{CeO}_2$  particles that were  
430 agglomerated.

431



432



433

Figure 5. SEM micrographs of  $Ce_xFe_yO$  ( $x:y=3:7$ ) after several tests. (a)~(e)

434

represents the catalysts reacted for one, two, three, four, five times respectively. (f)

435

EDX results for the reacted catalysts.

436

Possible carbon deposition on the used catalysts was carried out with TPO

437

analysis and the results were showed in Fig.6. The weight increased at 250 °C to 550

438

°C, it might be caused by the oxidation of metallic Fe (a few of Fe particles exist

439

possibly, cannot be seen in XRD patterns in Fig.4) and  $Fe_3O_4$  to  $Fe_2O_3$ . With the

440

increase of recycle times, the weight gaining of used catalysts shown in Fig.6 was

441

decreased. As part of the  $Fe_3O_4$  was oxidized to  $Fe_2O_3$  in the lifetime test as shown in

442

Fig.4. Therefore it cost less oxygen in the TPO test and resulted in less weight gain.

443

As for the oxidation peak shifting to higher temperature, it might be ascribed to the

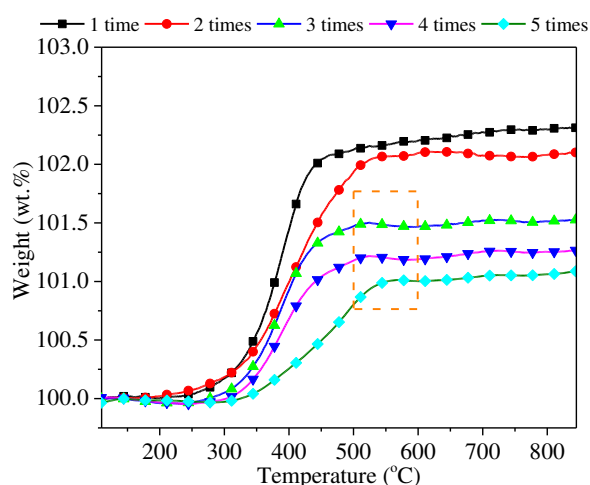
444

thermal sinter of  $Fe_3O_4$  particles after each recycle, which made  $Fe_3O_4$  hard to be

445

oxidized. However, the weight loss peak can be hardly seen in TPO analysis, only a

446 slight decrement was around 550 °C, it might be the oxidation of filamentous carbon  
447 [11, 48] and there was no amorphous carbon oxidizing peak. Generally speaking, the  
448 carbon deposition on catalysts was trace amounts and could be neglected. It seems  
449 that the presence of CeO<sub>2</sub> not only improved the oxidative ability of the iron catalysts,  
450 but was also in favour of the oxidation of possible deposited carbon on the surface of  
451 the used catalysts, because the CeO<sub>2</sub> has a high capacity and mobility of oxygen.



452

453 Figure 6. Temperature programmed oxidation of used catalysts after several  
454 recycles.

455

### 456 3.3 Influence of reaction temperature

457 The influence of catalytic temperature on the hydrogen production from biomass  
458 gasification was investigated, when cellulose pyrolysis temperature was kept at 800  
459 °C and the water feeding rate was 0.1 g min<sup>-1</sup> in the presence of the catalyst  
460 (Ce:Fe=3:7), while the gasification temperature varied from 500 °C to 900 °C at the  
461 step of 100 °C. As can be seen in Table 3, the gas yield was increased straightly from  
462 62.92 wt.% to 85.84 wt.%, which indicated that the gasification temperature had a

463 significant effect on the thermal conversion of liquid oil compounds to light gases.  
 464 For that gas product, the concentrations of hydrogen and carbon oxide increased  
 465 slightly as temperature increasing from 500°C to 700°C, while the content of methane  
 466 decreased straightly from 16.95 vol.% to 12.24 vol.%, but no obvious change showed  
 467 for carbon monoxide. This can be explained by that the increase of temperature  
 468 restrained the production of CH<sub>4</sub> while promoted the water gas shift reaction ( CO +  
 469 H<sub>2</sub>O = CO<sub>2</sub> + H<sub>2</sub> ). When the temperature was further increased to 800 °C, the yield of  
 470 hydrogen reached the maximum at 28.58 mmol and the concentration of CO was  
 471 increased significantly to 43.26 vol.%. These can be attributed to that the cracking  
 472 reactions and catalytic steam reforming of volatiles were enhanced with the increase  
 473 of reaction temperature. While at 900 °C, the yields of CO<sub>2</sub> and H<sub>2</sub> were decreased  
 474 while the yield of CO was increased at higher temperature, it might be iron's role on  
 475 reversed water gas shift (CO<sub>2</sub> + H<sub>2</sub> = CO + H<sub>2</sub>O) prevail over the former at elevated  
 476 temperature.

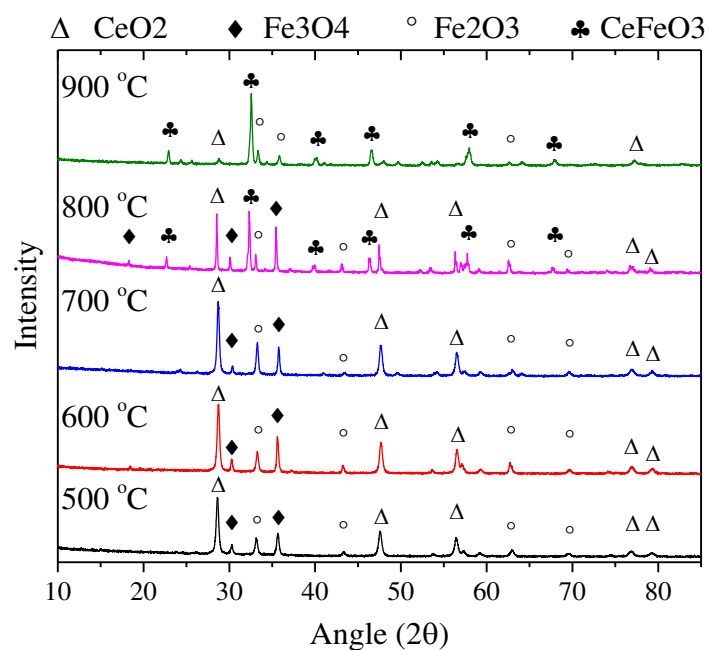
477 Table 3. The influence of gasification temperature on gas production.

Different gasification temperature (°C)	500	600	700	800	900
Gas yield (wt.%)	62.92	67.69	72.94	84.64	85.84
Mass balance (%)	102.92	99.53	97.01	98.30	97.88
H <sub>2</sub> yield (mmol g <sup>-1</sup> cellulose)	18.77	21.36	24.03	28.58	27.01
Gas composition (vol.%)					
H <sub>2</sub>	30.56	32.78	33.86	33.69	31.57
CO <sub>2</sub>	15.33	17.64	17.56	12.12	11.23
CH <sub>4</sub>	16.95	12.78	12.24	10.93	12.81
CO	37.16	36.80	36.35	43.26	44.40

478

479 Fig. 7 shows the results of XRD analysis of the used catalysts obtained at

480 different reaction temperatures. After used at 500 °C, a diffraction peak of Fe<sub>3</sub>O<sub>4</sub> was  
 481 showed with some Fe<sub>2</sub>O<sub>3</sub> and CeO<sub>2</sub>. With gasification temperature increasing from  
 482 500 to 700 °C, the diffraction peak of Fe<sub>3</sub>O<sub>4</sub> was increasing while the Fe<sub>2</sub>O<sub>3</sub> patterns  
 483 decreased; it indicated that proper high temperature was benefit for the reduction of  
 484 Fe<sub>2</sub>O<sub>3</sub> to Fe<sub>3</sub>O<sub>4</sub>. It should be notice that some CeFeO<sub>3</sub> patterns showed at 800 °C,  
 485 while Fe<sub>2</sub>O<sub>3</sub> and CeO<sub>2</sub> diminished. And when the temperature reached 900 °C, the  
 486 diffraction of CeFeO<sub>3</sub> becomes more remarkable while the diffraction patterns of  
 487 Fe<sub>3</sub>O<sub>4</sub> was disappeared. The peak of CeO<sub>2</sub> become weak and they are mainly existed  
 488 in CeFeO<sub>3</sub> with trace Fe<sub>2</sub>O<sub>3</sub>. It indicates that temperature was an important factor for  
 489 the formation of CeFeO<sub>3</sub>; CeO<sub>2</sub> would agglomerated with Fe<sub>2</sub>O<sub>3</sub> and formed CeFeO<sub>3</sub>  
 490 at higher temperature. The decrease of the diffraction of Fe<sub>3</sub>O<sub>4</sub> might be due to the  
 491 following two reasons; 1) More Fe ions were used to form CeFeO<sub>3</sub> lattice. 2) The  
 492 oxidation of Fe<sub>3</sub>O<sub>4</sub> to Fe<sub>2</sub>O<sub>3</sub> was enhanced at higher temperature.



493

494 Figure 7. XRD patterns of used catalysts (Ce:Fe=3:7) under different temperature.

495

#### 496 4. Conclusions

497 The present study introduced Ce/Fe catalyst into the biomass steam gasification.  
498 The influences of mole ratio of Ce:Fe and catalytic temperature on hydrogen  
499 production were investigated in a two stage gasification system. The main conclusions  
500 are listed as the follows. The CeO<sub>2</sub>/Fe<sub>2</sub>O<sub>3</sub> catalyst with a Ce:Fe ratio of 3:7 is optimal  
501 for the hydrogen production in cellulose steam gasification. When the temperature  
502 increased from 500 °C to 900 °C, the catalyst promoted the volatile steam gasification  
503 and resulted in the increasing of gas yield. However the highest hydrogen production  
504 was 28.58 mmol g<sup>-1</sup> cellulose at 800 °C owing to that the iron enhanced the reversed  
505 water shift reaction at 900 °C and caused the decreasing of hydrogen and carbon  
506 monoxide. CeFeO<sub>3</sub> can be generated at 800 °C or higher temperature after steam  
507 gasification of biomass without forming CeO<sub>2</sub>/Fe<sub>2</sub>O<sub>3</sub> clathrate. And the existence of  
508 CeFeO<sub>3</sub> enhanced the thermal stability of Ce/Fe catalyst. The increase of iron addition  
509 resulted in an enhancement of the crystallinity and the particle size of the used  
510 catalyst. The decrease of CeFeO<sub>3</sub> and Fe<sub>3</sub>O<sub>4</sub> rather than the agglomeration of CeO<sub>2</sub> or  
511 carbon deposition is the main reason that deactivated the catalysts in the lifetime test.  
512 The presence of CeO<sub>2</sub> not only improved the oxidative ability of the iron catalysts, but  
513 was also promoted the oxidation of possible deposited carbon on the surface of the  
514 used catalysts due to the high capacity and mobility of oxygen in CeO<sub>2</sub>.

515

#### 516 Acknowledgment

517 Financial support from the National Natural Science Foundation of China (Project  
518 No. 51622604) is greatly acknowledged. And many thanks to the technicians in  
519 Analytical & Testing Center of Huazhong University of Science and Technology. This  
520 work is also supported by Foundation of State Key Laboratory of Coal Combustion  
521 (FSKLCCA1805).

522

## 523 References

- 524 [1] M. Pehnt. Assessing future energy and transport systems: The case of fuel cells -  
525 Part 2: Environmental performance. *International Journal of Life Cycle Assessment*. 8  
526 (2003) 365-78.
- 527 [2] G. Chen, J. Andries, H. Spliethoff. Catalytic pyrolysis of biomass for hydrogen  
528 rich fuel gas production. *Energy Conversion and Management*. 44 (2003) 2289-96.
- 529 [3] L.H. Zhang, C.B. Xu, P. Champagne. Overview of recent advances in  
530 thermo-chemical conversion of biomass. *Energy Conversion and Management*. 51  
531 (2010) 969-82.
- 532 [4] J. Li, Y.Q. Chen, H.P. Yang, D.C. Zhu, X. Chen, X.H. Wang, et al. Correlation of  
533 Feedstock and Bio-oil Compound Distribution. *Energy & Fuels*. 31 (2017) 7093-100.
- 534 [5] E. Shayan, V. Zare, I. Mirzaee. Hydrogen production from biomass gasification; a  
535 theoretical comparison of using different gasification agents. *Energy Conversion and*  
536 *Management*. 159 (2018) 30-41.
- 537 [6] W.N. Li, Q.H. Li, R. Chen, Y. Wu, Y.G. Zhang. Investigation of hydrogen  
538 production using wood pellets gasification with steam at high temperature over 800  
539 degrees C to 1435 degrees C. *International Journal of Hydrogen Energy*. 39 (2014)  
540 5580-8.
- 541 [7] H.Y. Chu, Q.H. Li, A.H. Meng, Y.G. Zhang. Investigation of hydrogen production  
542 from model bio-syngas with high CO<sub>2</sub> content by water-gas shift reaction.  
543 *International Journal of Hydrogen Energy*. 40 (2015) 4092-100.
- 544 [8] T. Tian, Q.H. Li, R. He, Z.C. Tan, Y.G. Zhang. Effects of biochemical composition  
545 on hydrogen production by biomass gasification. *International Journal of Hydrogen*  
546 *Energy*. 42 (2017) 19723-32.
- 547 [9] J.G. Olsson, J.B. Pettersson, N. Padban, I. Bjerle. Alkali metal emission from filter  
548 ash and fluidized bed material from PFB gasification of biomass. *Energy & fuels*. 12  
549 (1998) 626-30.
- 550 [10] C. Wu, P.T. Williams. Hydrogen production by steam gasification of  
551 polypropylene with various nickel catalysts. *Applied Catalysis B-Environmental*. 87  
552 (2009) 152-61.
- 553 [11] C. Wu, P.T. Williams. Investigation of Ni-Al, Ni-Mg-Al and Ni-Cu-Al catalyst

554 for hydrogen production from pyrolysis-gasification of polypropylene. *Applied*  
555 *Catalysis B-Environmental*. 90 (2009) 147-56.

556 [12] C.F. Wu, P.T. Williams. Hydrogen Production from the Pyrolysis-Gasification of  
557 Polypropylene: Influence of Steam Flow Rate, Carrier Gas Flow Rate and  
558 Gasification Temperature. *Energy & Fuels*. 23 (2009) 5055-61.

559 [13] L.Y. Wei, H.P. Yang, B. Li, X.T. Wei, L. Chen, J.G. Shao, et al.  
560 Absorption-enhanced steam gasification of biomass for hydrogen production: Effect  
561 of calcium oxide addition on steam gasification of pyrolytic volatiles. *International*  
562 *Journal of Hydrogen Energy*. 39 (2014) 15416-23.

563 [14] C. Wu, Z. Wang, J. Huang, P.T. Williams. Pyrolysis/gasification of cellulose,  
564 hemicellulose and lignin for hydrogen production in the presence of various  
565 nickel-based catalysts. *Fuel*. 106 (2013) 697-706.

566 [15] P.H. Blanco, C. Wu, P.T. Williams. Influence of Ni/SiO<sub>2</sub> catalyst preparation  
567 methods on hydrogen production from the pyrolysis/reforming of refuse derived fuel.  
568 *International Journal of Hydrogen Energy*. 39 (2014) 5723-32.

569 [16] N. Laosiripojana, W. Sutthisripok, S. Charojrochkul, S. Assabumrungrat.  
570 Conversion of biomass tar containing sulphur to syngas by GdCeO<sub>2</sub> coated NiFe  
571 bimetallic-based catalysts. *Applied Catalysis A: General*. 478 (2014) 9-14.

572 [17] A. Laobuthee, C. Veranitisagul, W. Wattanathana, N. Koonsaeng, N.  
573 Laosiripojana. Activity of Fe supported by Ce<sub>1-x</sub>Sm<sub>x</sub>O<sub>2-δ</sub> derived from metal  
574 complex decomposition toward the steam reforming of toluene as biomass tar model  
575 compound. *Renewable Energy*. 74 (2015) 133-8.

576 [18] S.W. Luo, L. Zeng, L.S. Fan. Chemical Looping Technology: Oxygen Carrier  
577 Characteristics. in: J.M. Prausnitz, (Ed.). *Annual Review of Chemical and*  
578 *Biomolecular Engineering*, Vol 6. Annual Reviews, Palo Alto, 2015. pp. 53-75.

579 [19] M. Keller, H. Leion, T. Mattisson, H. Thunman. Investigation of Natural and  
580 Synthetic Bed Materials for Their Utilization in Chemical Looping Reforming for Tar  
581 Elimination in Biomass-Derived Gasification Gas. *Energy & Fuels*. 28 (2014)  
582 3833-40.

583 [20] M. Keller, H. Leion, T. Mattisson. Use of CuO/MgAl<sub>2</sub>O<sub>4</sub> and  
584 La<sub>0.8</sub>Sr<sub>0.2</sub>FeO<sub>3</sub>/γ-Al<sub>2</sub>O<sub>3</sub> in chemical looping reforming system for tar removal from  
585 gasification gas. *Aiche J.* (2015).

586 [21] M. Keller, H. Leion, T. Mattisson. Chemical looping tar reforming using  
587 La/Sr/Fe-containing mixed oxides supported on ZrO<sub>2</sub>. *Applied Catalysis B:*  
588 *Environmental*. 183 (2016) 298-307.

589 [22] G. Chen, J. Yao, J. Liu, B. Yan, R. Shan. Biomass to hydrogen-rich syngas via  
590 catalytic steam gasification of bio-oil/biochar slurry. *Bioresource Technology*. 198  
591 (2015) 108-14.

592 [23] Z. Huang, F. He, Y.P. Feng, K. Zhao, A.Q. Zheng, S. Chang, et al. Synthesis gas  
593 production through biomass direct chemical looping conversion with natural hematite  
594 as an oxygen carrier. *Bioresource Technology*. 140 (2013) 138-45.

595 [24] C. Lang, X. Secordel, Y. Zimmermann, A. Kiennemann, C. Courson.  
596 High-temperature Water-Gas Shift catalysts for hydrogen enrichment of a gas  
597 produced by biomass steam gasification. *Comptes Rendus Chimie*. 18 (2015) 315-23.

598 [25] G.K. Reddy, S.J. Kim, J.H. Dong, P.G. Smirniotis, J.B. Jasinski. Long-term WGS  
599 stability of Fe/Ce and Fe/Ce/Cr catalysts at high and low steam to CO ratios-XPS and  
600 Mossbauer spectroscopic study. *Applied Catalysis a-General*. 415 (2012) 101-10.  
601 [26] S. Cocchi, M. Mari, F. Cavani, J.-M.M. Millet. Chemical and physical behavior  
602 of CoFe<sub>2</sub>O<sub>4</sub> in steam-iron process with methanol. *Applied Catalysis B:  
603 Environmental*. 152–153 (2014) 250-61.  
604 [27] A. Khan, P. Chen, P. Boolchand, P.G. Smirniotis. Modified nano-crystalline  
605 ferrites for high-temperature WGS membrane reactor applications. *J Catal*. 253 (2008)  
606 91-104.  
607 [28] K. Svoboda, G. Slowinski, J. Rogut, D. Baxter. Thermodynamic possibilities and  
608 constraints for pure hydrogen production by iron based chemical looping process at  
609 lower temperatures. *Energy Conversion and Management*. 48 (2007) 3063-73.  
610 [29] M. Rafati, L.J. Wang, D.C. Dayton, K. Schimmel, V. Kabadi, A. Shahbazi.  
611 Techno-economic analysis of production of Fischer-Tropsch liquids via biomass  
612 gasification: The effects of Fischer-Tropsch catalysts and natural gas co-feeding.  
613 *Energy Conversion and Management*. 133 (2017) 153-66.  
614 [30] K.S. Kang, C.H. Kim, W.C. Cho, K.K. Bae, S.W. Woo, C.S. Park. Reduction  
615 characteristics of CuFe<sub>2</sub>O<sub>4</sub> and Fe<sub>3</sub>O<sub>4</sub> by methane; CuFe<sub>2</sub>O<sub>4</sub> as an oxidant for  
616 two-step thermochemical methane reforming. *International Journal of Hydrogen  
617 Energy*. 33 (2008) 4560-8.  
618 [31] G.K. Reddy, P. Boolchand, P.G. Smirniotis. Unexpected Behavior of Copper in  
619 Modified Ferrites during High Temperature WGS Reaction—Aspects of Fe<sup>3+</sup> ↔  
620 Fe<sup>2+</sup> Redox Chemistry from Mössbauer and XPS Studies. *J Phys Chem C*. 116 (2012)  
621 11019-31.  
622 [32] S.B. Bagherzadeh, M. Haghghi, N. Rahemi. Novel oxalate gel coprecipitation  
623 synthesis of ZrO<sub>2</sub>-CeO<sub>2</sub>-promoted CuO-ZnO-Al<sub>2</sub>O<sub>3</sub> nanocatalyst for fuel cell-grade  
624 hydrogen production from methanol: Influence of ceria-zirconia loading. *Energy  
625 Conversion and Management*. 134 (2017) 88-102.  
626 [33] D.H. Lee, K.S. Cha, Y.S. Lee, K.S. Kang, C.S. Park, Y.H. Kim. Effects of CeO<sub>2</sub>  
627 additive on redox characteristics of Fe-based mixed oxide mediums for storage and  
628 production of hydrogen. *International Journal of Hydrogen Energy*. 34 (2009)  
629 1417-22.  
630 [34] D. Yamaguchi, L.G. Tang, L. Wong, N. Burke, D. Trimm, K. Nguyen, et al.  
631 Hydrogen production through methane-steam cyclic redox processes with iron-based  
632 metal oxides. *International Journal of Hydrogen Energy*. 36 (2011) 6646-56.  
633 [35] Science-News. 2013 Runners-Up. Newcomer juices up the race to harness  
634 sunlight. *Science*. 342 (2013) 1438-9.  
635 [36] Nature-News-Features. 365 days: Nature's 10: Ten people who mattered this  
636 year-Henry Snaith: Sun worshipper. *Nature*. 504 (2013) 357-65.  
637 [37] A.M. Hafez, A.F. Zedan, S.Y. AlQaradawi, N.M. Salem, N.K. Allam.  
638 Computational study on oxynitride perovskites for CO<sub>2</sub> photoreduction. *Energy  
639 Conversion and Management*. 122 (2016) 207-14.  
640 [38] N.X. Lin, L.N. Huo, H.P. Liu, X. Fang, S.T. Wu, X. Chen, et al. Preparation and  
641 properties of pure crystalline perovskite CeFeO<sub>3</sub> thin films with vanadium doping. *J*

642 Am Ceram Soc. 100 (2017) 2932-8.  
643 [39] E.A. Zaboeva, S.G. Izotova, V.I. Popkov. Glycine-Nitrate Combustion Synthesis  
644 of CeFeO<sub>3</sub>-based Nanocrystalline Powders. Russ J Appl Chem+. 89 (2016) 1228-36.  
645 [40] L.L. Petschnig, G. Fuhrmann, D. Schildhammer, M. Tribus, H. Schottenberger, H.  
646 Huppertz. Solution combustion synthesis of CeFeO<sub>3</sub> under ambient atmosphere.  
647 Ceram Int. 42 (2016) 4262-7.  
648 [41] N.R. Manwar, R.G. Borkar, R. Khobragade, S.S. Rayalu, S.L. Jain, A.K.  
649 Bansiwala, et al. Efficient solar photo-electrochemical hydrogen generation using  
650 nanocrystalline CeFeO<sub>3</sub> synthesized by a modified microwave assisted method.  
651 International Journal of Hydrogen Energy. 42 (2017) 10931-42.  
652 [42] T.R. Sahoo, M. Armandi, R. Arletti, M. Piumetti, S. Bensaid, M. Manzoli, et al.  
653 Pure and Fe-doped CeO<sub>2</sub> nanoparticles obtained by microwave assisted combustion  
654 synthesis: Physico-chemical properties ruling their catalytic activity towards CO  
655 oxidation and soot combustion. Applied Catalysis B-Environmental. 211 (2017)  
656 31-45.  
657 [43] J. Zou, H. Yang, Z. Zeng, C. Wu, P.T. Williams, H. Chen. Hydrogen production  
658 from pyrolysis catalytic reforming of cellulose in the presence of K alkali metal.  
659 International Journal of Hydrogen Energy. 41 (2016) 10598-607.  
660 [44] J. Wang, C.Y. Han, X.Y. Gao, J.C. Lu, G.P. Wan, D.D. He, et al. Rapid synthesis  
661 of Fe-doped CuO-Ce(0.8)Zr(0.2)O(2) catalysts for CO preferential oxidation in  
662 H<sub>2</sub>-rich streams: Effect of iron source and the ratio of Fe/Cu. Journal of Power  
663 Sources. 343 (2017) 437-45.  
664 [45] O. Vozniuk, S. Agnoli, L. Artiglia, A. Vassoi, N. Tanchoux, F. Di Renzo, et al.  
665 Towards an improved process for hydrogen production: the chemical-loop reforming  
666 of ethanol. Green Chemistry. 18 (2016) 1038-50.  
667 [46] A. Khan, P.G. Smirniotis. Relationship between temperature-programmed  
668 reduction profile and activity of modified ferrite-based catalysts for WGS reaction. J  
669 Mol Catal a-Chem. 280 (2008) 43-51.  
670 [47] L.F. Zhang, Y.X. Wu. Sol-Gel Synthesized Magnetic MnFe<sub>2</sub>O<sub>4</sub> Spinel Ferrite  
671 Nanoparticles as Novel Catalyst for Oxidative Degradation of Methyl Orange. J  
672 Nanomater. 2013 (2013).  
673 [48] D.D. Yao, Y.S. Zhang, P.T. Williams, H.P. Yang, H.P. Chen. Co-production of  
674 hydrogen and carbon nanotubes from real-world waste plastics: Influence of catalyst  
675 composition and operational parameters. Applied Catalysis B-Environmental. 221  
676 (2018) 584-97.  
677